Taylor & Francis
Taylor & Francis Group

Canadian Journal of Remote Sensing
Journal canadien de télédétection

ISSN: (Print) (Online) Journal homepage: https://www.tandfonline.com/loi/ujrs20

Intelligent Sine Cosine Optimization with Deep Transfer Learning Based Crops Type Classification Using Hyperspectral Images

José Escorcia-Gutierrez, Margarita Gamarra, Melitsa Torres-Torres, Natasha Madera, Juan C. Calabria-Sarmiento & Romany F. Mansour

To cite this article: José Escorcia-Gutierrez, Margarita Gamarra, Melitsa Torres-Torres, Natasha Madera, Juan C. Calabria-Sarmiento & Romany F. Mansour (2022): Intelligent Sine Cosine Optimization with Deep Transfer Learning Based Crops Type Classification Using Hyperspectral Images, Canadian Journal of Remote Sensing, DOI: 10.1080/07038992.2022.2081538

To link to this article: https://doi.org/10.1080/07038992.2022.2081538

CANADIAN JOURNAL OF REMOTE SENSING
https://doi.org/10.1080/07038992.2022.2081538

Taylor & Francis
Taylor & Francis Group

Intelligent Sine Cosine Optimization with Deep Transfer Learning Based Crops Type Classification Using Hyperspectral Images

Optimisation intelligente du sinus-cosinus et classification des types de cultures basée sur l'apprentissage par transfert profond à l'aide d'images hyperspectrales

José Escorcia-Gutierrez[a,b], Margarita Gamarra[c], Melitsa Torres-Torres[d], Natasha Madera[e], Juan C. Calabria-Sarmiento[f,g], and Romany F. Mansour[h]

[a]Biomedical Engineering Program, Corporación Universitaria Reformada, Barranquilla 080001, Colombia; [b]Research Center - CIENS, Escuela Naval de Suboficiales A.R.C. "Barranquilla", Barranquilla 080001, Colombia; [c]Departament of Computational Science and Electronic, Universidad de la Costa, CUC, Barranquilla 08001, Colombia; [d]Research Group IET-UAC, Universidad Autónoma del Caribe, Barranquilla 08001, Colombia; [e]Electronics and Telecommunications Engineering Program, Universidad Autónoma del Caribe, Barranquilla 080001, Colombia; [f]Department of Computer Science, Universidad Simon Bolivar, Barranquilla 080001, Colombia; [g]Doctorate in Computer Science, Universidad del Norte, Barranquilla 080001, Colombia; [h]Department of Mathematics, Faculty of Science, New Valley University, El-Kharga 72511, Egypt

ABSTRACT

Hyperspectral Remote Sensing (HRS) is an emergent, multidisciplinary paradigm with several applications, which are developed on the basis of material spectroscopy, radiative transfer, and imaging spectroscopy. HRS plays a vital role in agriculture for crops type classification and soil prediction. The recently developed artificial intelligence techniques can be used for crops type classification using HRS. This study develops an Intelligent Sine Cosine Optimization with Deep Transfer Learning Based Crop Type Classification (ISCO-DTLCTC) model. The ISCO-DTLCTC technique comprises initial preprocessing step to extract the region of interest. The information gain-based feature reduction technique is employed to reduce the dimensionality of the original hyperspectral images. In addition, a fusion of 3 deep convolutional neural networks models namely, VGG16, SqueezeNet, and Dense-EfficientNet perform feature extraction process. Furthermore, sine cosine optimization (SCO) algorithm with Modified Elman Neural Network (MENN) model is applied for crops type classification. The design of SCO algorithm helps to proficiently select the parameters involved in the MENN model. The performance validation of the ISCO-DTLCTC model is carried out using benchmark datasets and the results are inspected under several measures. Extensive comparative results demonstrated the betterment of the ISCO-DTLCTC model over the state of art approaches with maximum accuracy of 99.99%.

RÉSUMÉ

La télédétection hyperspectrale (HRS) est une technologie émergente et multidisciplinaire ayant plusieurs applications développées sur la base de la spectroscopie des matériaux, du transfert radiatif et de la spectroscopie des images. L'HRS joue un rôle essentiel en agriculture pour la classification des types de cultures et la prévision des sols. Les techniques d'intelligence artificielle (IA) récemment développées peuvent être utilisées pour la classification des types de cultures à l'aide de HRS. Cette étude développe un modèle intelligent d'optimisation du sinus-cosinus avec une classification des types de cultures basée sur l'apprentissage par transfert profond (ISCO-DTLCTC). La technique ISCO-DTLCTC comprend une étape initiale de prétraitement pour extraire la région d'intérêt (RoI). La technique IGFR (Information Gain Based Feature Reduction) est utilisée pour réduire la dimensionnalité des images hyperspectrales originales. Une fusion de trois modèles DCNN (Deep Convolutional Neural Networks), à savoir VGG16, SqueezeNet et Dense-EfficientNet, effectue un processus d'extraction des principales caractéristiques. En outre, l'algorithme d'optimisation du sinus-cosinus (SCO) avec le modèle MENN (Modified Elman Neural Network) est appliqué à la classification des types de cultures. La conception de l'algorithme SCO permet de sélectionner efficacement les paramètres impliqués dans le modèle MENN. La validation des performances du modèle ISCO-DTLCTC est effectuée à l'aide d'ensembles de données de référence et

ARTICLE HISTORY
Received 16 February 2022
Accepted 15 May 2022

CONTACT José Escorcia-Gutierrez jose.escorcia23@gmail.com

les résultats sont validés avec différents paramètres. Les résultats démontrent l'efficacité du modèle ISCO-DTLCTC par rapport aux approches de pointe avec une précision maximale de 99,99%.

Introduction

Recently, people have started to acquire hyperspectral remote sensing (HRS) images using higher spectral resolution and higher spatial resolution quite easily (Singh et al. 2020). Since HRS imaging has stronger solving power for fine spectra, they have wide-ranging applications (Jamali et al. 2021) in military, environmental, medical, and mining areas. The acquisition of hyperspectral remote sensing image based on imaging spectrometer deployed in distinct spaces. It is utilized for images in the visible, ultraviolet, mid-infrared, and near-infrared regions of electromagnetic waves. The imaging spectrometer could image is very narrow and has many continuous bands, hence all the pixels in the wavelength range could get a fully emitted or reflected spectrum (Chasmer et al. 2022). Thus, a hyperspectral image has the feature of abundant data, higher spectral resolution, and many bands. The processing method of hyperspectral remote sensing images primarily includes transformation, image correction, dimension reduction, classification, and noise reduction (Meneghini et al. 2022). Different from normal images, hyperspectral image is rich in spectral data, and that reflects the chemical composition and physical structure of the object of interest that is useful for image classification. Hyperspectral image classification is the active part of the study in the hyperspectral fields (Lu et al. 2020).

Hyperspectral (HS) image classification often suffered from variety of artifacts, namely, limited or unbalanced training samples, high dimensionality, mixing pixels, and spectral variability. The Hughes phenomenon is a common challenge in the supervised classification method (Uddin et al. 2021). The power of classification increased with an increasing training sample. The limited accessibility of the training sample reduces the classification accuracy with the increasing feature dimension. Such effect is called as "Hughes phenomenon" (Thenkabail et al. 2019). It is familiar that high redundancy and increased data dimension among features may create problems at the time of data analysis. Several considerable problems should be resolved while implementing hyperspectral image classification. Over the last few years, deep learning technique has rapidly established and gained considerable interest.

In comparison with the conventional machine learning method (ML), deep learning (DL) technique does not need to artificially design feature patterns and could automatically learn patterns from data. Thus, it has been applied effectively in the field of speech recognition, NLP, autonomous driving, object detection, and semantic segmentation, and gained outstanding performance. In recent times, it has been presented in the fields of HRI classification. The researcher presented many new DL-based HRS classification methods. HRS images play a vital role in agricultural processes and are utilized to crop condition observing, agricultural yield estimating, pest observing, etc. During the agricultural surveys, the fine classifier of HRI offers the info of crops distributing (Papp et al. 2021; Mansour et al. 2021). Fine classifiers of crops need images with higher spatial and spectral resolution (Lassalle 2021; Ang and Seng 2021).

This study develops an Intelligent Sine Cosine Optimization with Deep Transfer Learning Based Crop Type Classification (ISCO-DTLCTC) model using HRI. The presented ISCO-DTLCTC technique involves information gain-based feature reduction (IGFR) technique to reduce the dimensionality of the original hyperspectral images. Also, a fusion of 3 deep convolutional neural networks (DCNN) models, namely, VGG16, SqueezeNet, and Dense-EfficientNet models perform feature extraction process. Finally, sine cosine optimization (SCO) algorithm with modified Elman Neural Network (MENN) model is applied for crop type classification. The performance validation of the ISCO-DTLCTC model is carried out using benchmark dataset and the results are inspected under several measures.

Related works

The authors in (Bhosle and Musande 2019) aimed in examining utilize of DL-CNN for LULC classifier on Indian Pines data set and for crop identifying on our survey region data set. During the existing works, AVIRIS sensor's Indian Pines standard data set was utilized for LULC classifier. The study region from Phulambri, Aurangabad, MH, India, was utilized as to crop classifier. Wei et al. (2021) presented a fine classifier technique dependent upon multifeature fusion and DL. During this case, the morphological profiles,

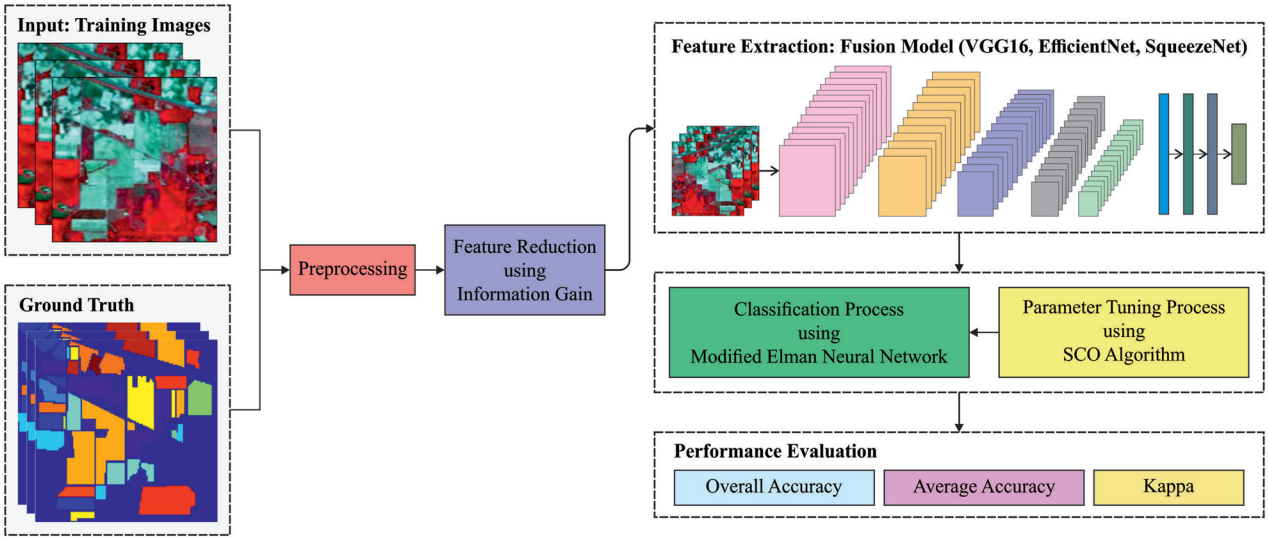

Figure 1. The overall process of ISCO-DTLCTC technique.

GLCM texture, and endmember abundance feature are leveraged for exploiting the spatial data of hyperspectral imagery. Next, several spatial data were fused with novel spectral data for generating classifier outcomes by utilizing the DNN with conditional random field (DNN + CRF) method. In detail, the DNN is a deep detection method that is extracting depth features and mine the possible data.

In Wan et al. (2021), a 2-phase classifier is designed for displaying the performance of the image classifier. Specifically, this analysis utilized a multiclass classifier by SVM + CNN for an image classifier analysis. SVM is a supervised learning method that analyzes data utilized to classifier. CNN is a class of DNNs that is executed for analyzing visual imagery. In Roy et al. (2021), a novel end-to-end morphological DL structure (named MorphConvHyperNet) was established. The presented method capably approaches non-linear data under the trained procedure of HSI classifier. Especially, this technique comprises spectral and spatial morphological blocks for extracting relevant features in the HSI input data.

Shi et al. (2021) presented a double-branch network containing a new convolutional called pyramidal convolutional (PyConv) and iterative attention process. All the branches focus on exploiting spectral-spatial features with distinct PyConvs, improved by the attention element to refine the feature map. In Sun et al. (2020), a spectral-spatial attention network (SSAN) was presented for capturing discriminative spectral-spatial features in attention regions of HSI cube. Primary, an easy spectral-spatial network (SSN) was created for extracting spectral-spatial features in HSI cubes. Secondary, an attention element was established for suppressing the effect of interfering pixels.

The proposed model

In this study, a new ISCO-DTLCTC technique has been developed for the detection and classification of crop types using HRSs. The presented ISCO-DTLCTC technique comprises different stages of subprocesses, namely, preprocessing, region of interest (RoI) extraction, IGFR-based feature reduction, fusion-based feature extraction, MENN-based crop classification, and SCO-based parameter optimization. Figure 1 illustrates the overall process of ISCO-DTLCTC technique.

Preprocessing

Thresholding was executed utilizing Otsu approach as it can be extremely utilized for estimating ROI in the image that comprises the crop region. The outcome of thresholding was feasible for containing the noise (the non-crop region that is categorized as the crop region). Individual noises were feasibly connected/unconnected to crop objects. For removing the noise, the morphology of functions is carried out (Zhao et al. 2020). Individual functions are opening and closing that are implemented successively utilizing disk-shaped structuring elements (strel). The opening function is needed for detaching the linked noise in the crop region, but the closing function is for combining and filling from the crop regions that are classified as background.

Feature reduction

Next to preprocessing, feature reduction process is performed using IGFR technique. It is mainly utilized on higher dimension information to estimate the efficacy of attributes in classification. IGFR measures the worth of attributes by estimating the IGFR of features regarding the targeted class (Singh and Singh 2021). Indeed, IGFR calculates the number of data needed for predicting the targeted class by knowing the absence or presence of an attribute. Consider the discrete arbitrary parameter y comprises 2 probable results. The binary entropy function H, shown in Shannon unit, that is, logarithmic base 2 is characterized by Equation (1), whereas p_i indicates the likelihood that arbitrary instance $y \in i$ amongst m classes in dataset D. p_i is assessed by $|y_{iD}|/|D|$.

$$H(y) = -\sum_{j-1}^{m} p_i \log_2(p_i) \tag{1}$$

In the course of making decision process, entropy quantifies the uncertainty of feature. The predicted data required to categorize sample y according to partitioning by a is evaluated by

$$\begin{aligned} H(Y|X) &= -\sum_{a\in X} p(a) \sum_{y\in Y} p(ya) \log_2 p(y|a) \\ &= -\sum_{a\in X} \sum_{y\in Y} p(a,\ y) \log_2 p(ya) \end{aligned} \tag{2}$$

$$lG(y|a) = H(y) - H(y|a) \tag{3}$$

Specifically, the IGFR for feature (a) is provided in Eq. (*Reject* whereby marginal entropy is embodied as $H()$ and conditional entropy of y shown a is provided as $H(\gamma|a)$. The IGFR is a fast filter-based FS approach whereby the attribute is graded in descending order of IG score and is carefully chosen according to threshold. High IG implies better discriminatory power for making decisions (Singh and Singh 2021).

Feature extraction

During feature extraction process, a fusion of 3 DL models, namely, VGG16, SqueezeNet, and DenseEfficientNet models are carried out (Talkhabi et al. 2022; Nayak et al. 2022; Bernardo et al. 2021). VGG-16 is the best network configuration amongst the VGGNet constructed by the VGG group. VGG-16 (VGGNet) accomplished accuracy of 92.7% in the ImageNet ILSVRC2014. Because of its high accuracy and uniform structure in classification tasks. VGG-16 has a deep network when compared to AlexNet and comprises 16 trained layers together with 13 convolution layers and 3 FC layers. The model features a smooth and homogeneous structure that employs filter of size 2×2 pooling with a stride of 2 in each layer and 3×3 with a stride of 1 for convolution. The amount of convolutional filter remains same within one block and doubles afterward max-pooling layer from 64 in the first block to 512 in the latter block.

A dense CNN model is a mixture of pretrained EfficientNetB0 with dense layer. EfficientB0 has 7 MBConv blocks and 230 layers. It features a thick block structure comprising 4 closely connected layers with a growth rate of 4. Each layer uses the output feature map of the previous level as the input feature map. The dense block concept is comprised of convolutional layer of the same size as input feature maps in EfficientNet. The dense block uses previous convolutional layer output feature map for generating more feature maps with some convolutional kernel. The dense EfficientNet has an alternative dense and drop-out layer. A dense layer is an elementary layer that feeds each output from the preceding layer to neuron, all the neurons provide 1 output to the following layer. The drop-out layer is utilized for reducing the capacity or thinning the network at the time of training and avoiding over-fitting. Then, add a pooling layer, 3 drop-out layers, and 4 dense layers for ensuring the model work efficiently, the author has utilized a dense layer composed of 4 FC neurons in combination with a Softmax output layer to classify and compute the probability score for all the classes.

SqueezeNet is an 18-layer DNN designed with a small amount of parameters, still maintaining a higher accuracy. The usage of SqueezeNet assists in reducing the processing time and the memory consumption for classification than other multi-layer DL models. They selected the SqueezeNet architecture because of its lightweight structure, faster training times, and small amount of parameters. SqueezeNet is more commonly utilized by researchers for different applications. The major benefit of the SqueezeNet architecture is a fifty times performance improvement over AlexNet, a standard deep CNN architecture while maintaining a comparable classification performance. To guarantee computation efficacy, the size of convolutional filter has been minimized from 3×3 to 1×1. Consequently, the amount of trained parameters has been minimized by 9 times. Therefore, the SqueezeNet architecture is constructed from module of a similar type, named "Fire module". A Fire module encompasses of squeeze convolutional layer (that has 1×1 filter) that feeds into an expanded layer that has a mixture of 1×1 and 3×3 convolutional filters.

Here, the fusion of 3 DL models takes place for computing a set of feature vectors. They demonstrates as follows.

$$f_{GLCM1\times n} = \{VGG16_{1\times 1},\ VGG16_{1\times 2},\ VGG16_{1\times 3},\ \cdots,\ VGG16_{1\times n}\} \tag{4}$$

$$f_{\mathrm{DEFN}1\times l} = \{DEFN_{1\times 1},\ DEFN_{1\times 2},\ DEFN_{1\times 3},\ \cdots,\ DEFN_{1\times l}\}$$

$$f_{SN\times m} = \{SN_{1\times 1},\ SN_{1\times 2},\ SN_{1\times 3},\ \cdots, SN_{1\times n}\} \tag{5}$$

Then, the resultant feature is combined as to individual vector, as provided under.

$$\begin{aligned} &Fused(features\ \ vector)1\times \mathrm{q} \\ &= \sum\nolimits_{i=1}^{3}\{f_{GLCM1\times n}, f_{\mathrm{DEFN}1\times l},\}\ f_{SN\times m} \end{aligned} \tag{6}$$

where f is fused vector (1×1186).

Crop type classification

At the time of crop type classification, the MENN model (Song and Wang 2021) is applied to allocate proper class labels to it. The infrastructure of ENN was separated into 4 parts such as context unit, input state, hidden state, and resultant state. The input state is utilized for transmitting the raw data; introduced weighted data were mapped linearly or non-linearly with the transfer operation of hidden state; lastly, the processed data were carried out the linear weight approach from the resultant state. But, unlike BP-FFNN, ENN added further the context units for storing the resultant data of preceding moment of hidden state and feed-back it to next moment of hidden state (Song and Wang 2021). Therefore, this network not only improves the sensitivity to historic information but along has more dynamic data memory capability than the typical static network (Song and Wang 2021). The mathematical process of typical ENN infrastructure is summarized as:

$$y(t) = g(w_3 x(t)) \tag{7}$$

$$x(t) = f(w_1 x_c(t) + w_2(u(t-1)) \tag{8}$$

$$x_c(t) = x(t-1) \tag{9}$$

where $x(t)$, $y(t)$, $X(t)$ signifies the t^{th} resultant of hidden state, output state, and context unit, correspondingly. u refers to the input vector of input state. w_1, w_2, and w_3 signifies the connection weight of context units to hidden states, input to hidden states, and hidden to output states correspondingly. f and g define the transfer operation of hidden and output states correspondingly. Thus, to enhance the model efficiency of typical ENN, during this case, the MENN infrastructure is created. It not only accounts for the complete data feed-back in the hidden state, along with the data feedback in the context unit itself. Further relevant data are fed back to network and the instance data is examined further comprehensively which is further conducive to the last classifier. The mathematical process of MENN infrastructure is altered from the context unit as follows:

$$x_c(t) = \alpha \cdot x_c(t-1) + x(t-1) \tag{10}$$

where α refers to the scalar constant which modulates the weight of data feedback resultant in the context unit at the preceding moments. For $\alpha = 0$, the MENN infrastructure has essentially typical ENN method and has no memory of context units. Besides, the cross entropy was utilized as loss function and determined as follows:

$$\begin{aligned} L(d,\ y) = -\sum\nolimits_{j=1}^{N}[d_j(t)\ \log\ y_j(t) \\ + (1-d_j(t))\ \log\ (1-y_j(t))] \end{aligned} \tag{11}$$

where $d(t)$ refers to the target value of novel data and $y_j(t)$ has attained resultant value.

Parameter optimization

For optimal parameter selection of the MENN model, the SCO algorithm has been employed to accomplish enhanced crop classification performance. As with other swarm intelligence approaches, in the initialized phase of SCO algorithm, the population initialization is arbitrarily produced with the provided solution space, and the optimum solution is attained from the initialized population (Abualigah and Diabat 2021). The next is to repeat the procedure till the end criteria are attained. Initially, upgrade the adoptive parameter $r1$ and random parameters including 2, $r3$, and $r4$ are given in the following

$$\begin{aligned} r_1 &= a - t * \mathrm{a}/\mathrm{t}_{\max} \\ r_2 &= 2 * \pi * rand(\ ) \\ r_3 &= 2 * rand() \\ r_4 &= rand() \end{aligned} \tag{12}$$

Where as a is equivalent to 2; t and $t_{ma\times}$. mean the existing iteration and the maximal iteration, correspondingly; $rand0$ is utilized for producing the arbitrary value within$[0, 1]$, and π shows a constant. Next, the position of agent is upgraded as follows.

$$\mathrm{X}_{i,j}^{t+1} = \begin{cases} X_{i,j}^{T} + r_1 * \sin\ (r_2) * |r_3 * P_j^T - X_{i,j}^T| \\ X_{i,j}^{T} + r_1 * \cos\ (r_2) * |r_3 * P_j^T - X_{i,j}^T| \end{cases} \tag{13}$$

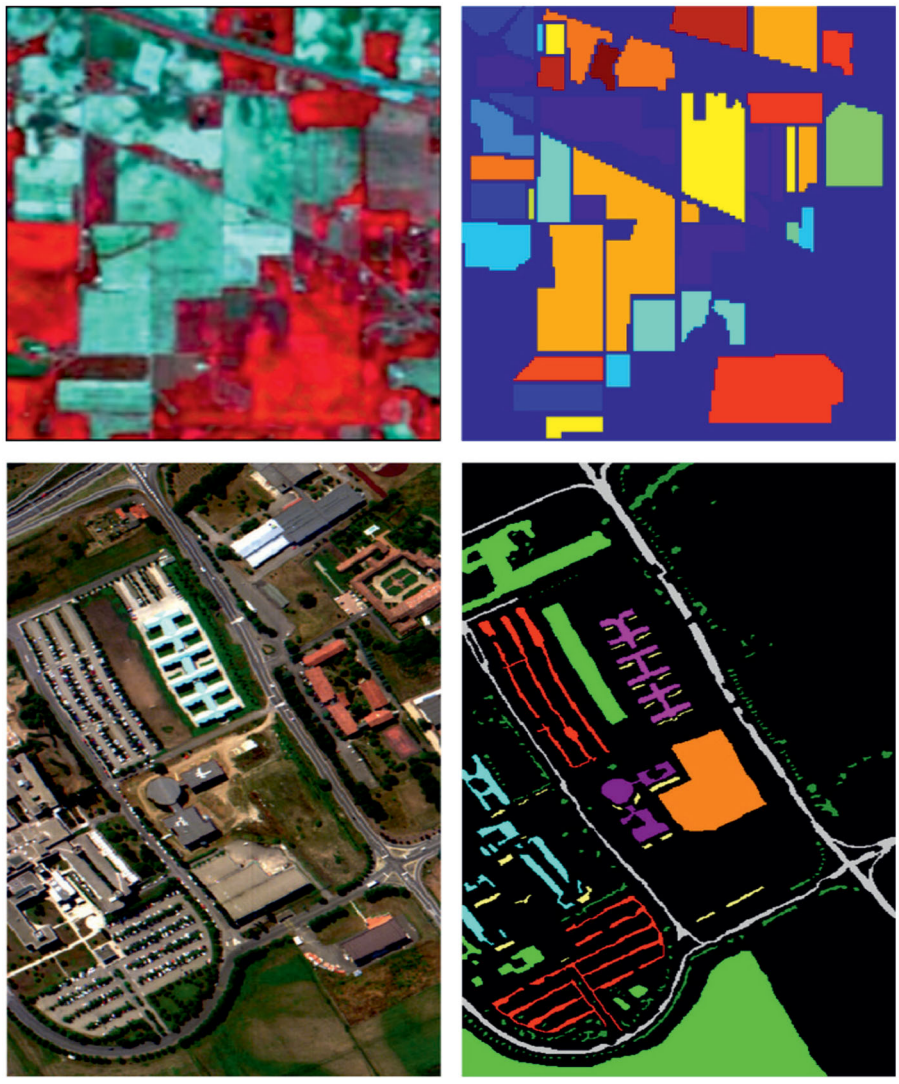

Figure 2. Sample images: (a) original image and (b) ground truth.

Here $X_{i,j}^{t+1}$ and $X_{i,j}^{t}$ indicates the *jth* parameter of *ith* agent at t th iteration and $(t+1)th$ iteration, correspondingly; and P_j^t implies the *jth* variable of optimum solution at the *tth* iteration. Lastly, the cross-border process is implemented to guarantee that each agent is in the potential region. When there is an agent i.e., superior to the optimum solution, the optimum solution is upgraded by this agent. The pseudocode of the fundamental SCO algorithm is given in Algorithm 1.

Algorithm 1. Pseudocode of SCO algorithm

Input: Population size, N; Problem dimension, D; Lower boundary, lb; the upper boundary, ub; the maximal iteration t_{max}
Output: Optimum solution P.
Arbitrarily initialize the population $X_i(i = 1, 2, ..., N)$ within limits, ub and lb, estimate the initialized population, attain the optimum solution P, $t = 1$.
while $t <= t_{max}$. do
Upgrade the parameter r_1.
for $i = 1$ *to* N
Upgrade the parameters r_2, r_3, and r_4.
Upgrade the location X_i.
end for
Amend the location of all the agents within the limits.
Estimate the existing population.
Upgrade the optimum solution P.

$$t = t + 1.$$

end while
Return the optimum solution P.

The SCO approach develops a FF for attaining enhanced classified performance. It resolves a positive integer for signifying an optimal performance of candidate solutions. During this case, the minimization

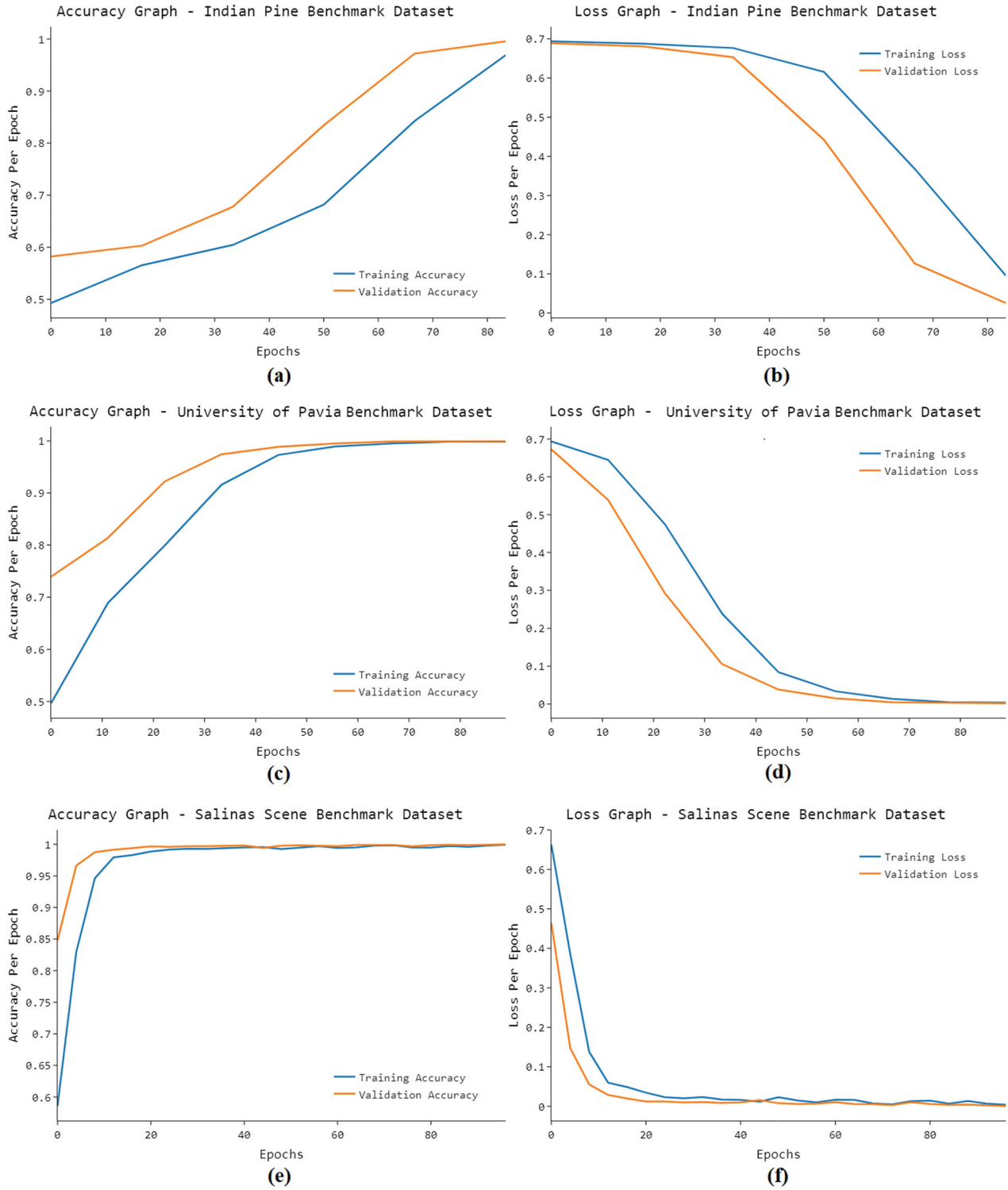

Figure 3. Result analysis of ISCO-DTLCTC technique under 3 datasets: (a) accuracy-INB dataset, (b) loss-INB dataset, (c) accuracy-UPB dataset, (d) loss-UPB dataset, (e) accuracy-SSB dataset, and (f) loss-SSB dataset.

of classifier error rate was assumed that FF is offered in Equation (14). Optimum solutions have a lower error rate and worst solution gains an enhanced error rate.

$$fitness(x_i) = ClassifierErrorRate(x_i) = \frac{number\ of\ misclassified\ images}{Total\ number\ of\ images} * 100 \quad [14]$$

Experimental validation

The performance validation of the ISCO-DTLCTC model is validated using the Indian Pines Benchmark (INB) (Kuo et al. 2014), University of Pavia Benchmark(UPB) (Luo et al. 2019), and Salinas Scene Benchmark (SSB) (http://www.ehu.eus/ccwintco/index.php/Hyperspectral_Remote_Sensing_Scenes). A few sample images are illustrated in Figure 2. The proposed model is simulated using Python tool and the results are investigated under varying sizes of training and testing data.

Figure 3 offers the accuracy and loss graph analysis of the ISCO-DTLCTC technique under 3 datasets. The outcomes outperformed that the accuracy value tends to increase and loss value tends to decrease with an increase in epoch count. It can be also observed that the training loss is low and validation accuracy is high technique under 3 datasets.

Table 1 and Figure 4 provide an overall crop classification outcomes of the ISCO-DTLCTC model on the test INB dataset under distinct training sizes (TSs). The experimental values indicated that the ISCO-DTLCTC model has resulted in enhanced classifier results under all TSs. For instance, with TS of 5%, the ISCO-DTLCTC model has provided OACC of 87.64%, AACC of 85.98%, and kappa of 83.69%.

Table 2 and Figure 5 offer an overall crop classification outcomes of the ISCO-DTLCTC model on the test UPB dataset under different TSs. The experimental values designated that the ISCO-DTLCTC approach has resulted in enhanced classifier results under all TSs. For instance, with TS of 5%, the ISCO-DTLCTC method has provided OACC of 98.41%, AACC of 97.73%, and kappa of 96.72%.

Table 3 and Figure 6 provide an overall crop classification outcomes of the ISCO-DTLCTC method on the test SAB dataset under distinct TSs. The experimental values exposed that the ISCO-DTLCTC approach has resulted in enhanced classifier results under all TSs. For instance, with TS of 5%, the ISCO-DTLCTC methodology has provided OACC of 99.21%, AACC of 99.11%, and kappa of 98.87%.

Table 4 reports the training time (TRT) and testing time (TST) inspection of the ISCO-DTLCTC model with existing technique.

Table 1. Result analysis of ISCO-DTLCTC technique under different training sizes on INB dataset.

Training Size (%)	Overall Accuracy (%)	Average Accuracy (%)	Kappa (%)_
5	87.64	85.98	83.69
10	95.23	94.45	93.51
15	98.97	98.19	97.77
20	99.39	99.13	98.76
25	99.85	99.59	99.39
30	99.96	99.85	99.54

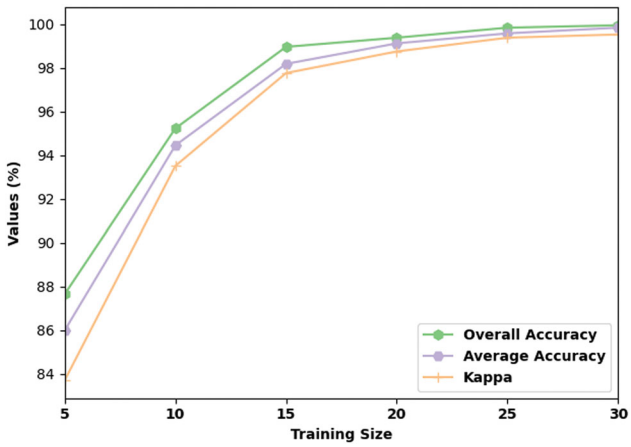

Figure 4. Result analysis of ISCO-DTLCTC technique on INB dataset.

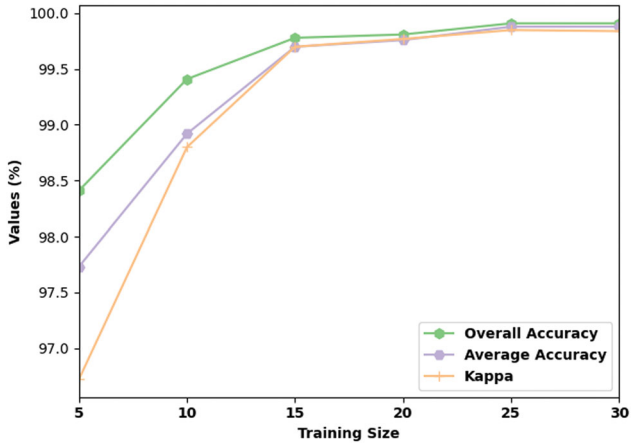

Figure 5. Result analysis of ISCO-DTLCTC technique under UPB dataset.

Table 2. Result analysis of ISCO-DTLCTC technique under different training sizes on UPB dataset.

Training Size (%)	Overall Accuracy	Average Accuracy	Kappa
5	98.41	97.73	96.72
10	99.41	98.92	98.80
15	99.78	99.70	99.70
20	99.81	99.76	99.77
25	99.91	99.88	99.85
30	99.91	99.88	99.84

Table 3. Result analysis of ISCO-DTLCTC technique under different training sizes on SAB dataset.

Training Size (%)	Overall Accuracy	Average Accuracy	Kappa
5	99.21	99.11	98.87
10	99.85	99.62	99.46
15	99.98	99.96	99.96
20	99.98	99.97	99.97
25	99.99	99.98	99.98
30	99.99	99.98	99.98

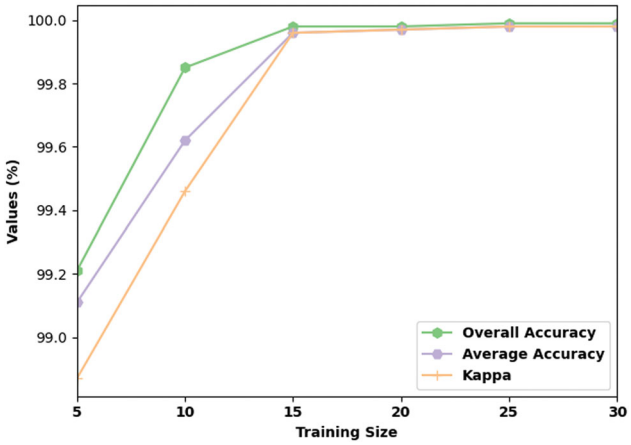

Figure 6. Result analysis of ISCO-DTLCTC technique under SAB dataset.

Table 4. Training and testing time analysis of ISCO-DTLCTC technique under 3 datasets.

Datasets	Methods	Training Time (s)	Testing Time (s)
INB dataset	HDSRN	570.00	3.00
	ISCO-DTLCTC	462.00	2.10
UPB dataset	HDSRN	940.00	8.00
	ISCO-DTLCTC	722.00	5.00
SAB dataset	HDSRN	930.00	8.00
	ISCO-DTLCTC	761.00	5.30

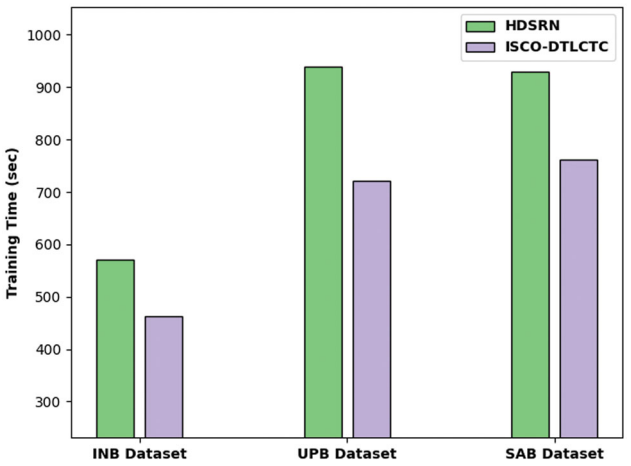

Figure 7. TRT analysis of ISCO-DTLCTC technique under 3 datasets.

Figure 7 portrays the comparative TRT examination of the ISCO-DTLCTC model with the existing HDSRN model. The figure indicated that the ISCO-DTLCTC model has accomplished enhanced outcomes with the minimal TRT under all datasets. For instance, with INB dataset, the ISCO-DTLCTC model has offered lower TRT of 462 seconds, whereas the HDSRN model has provided higher TRT of 470 seconds. Besides, with UPB dataset, the ISCO-DTLCTC approach has offered lesser TRT of 722 seconds, whereas the HDSRN approach has

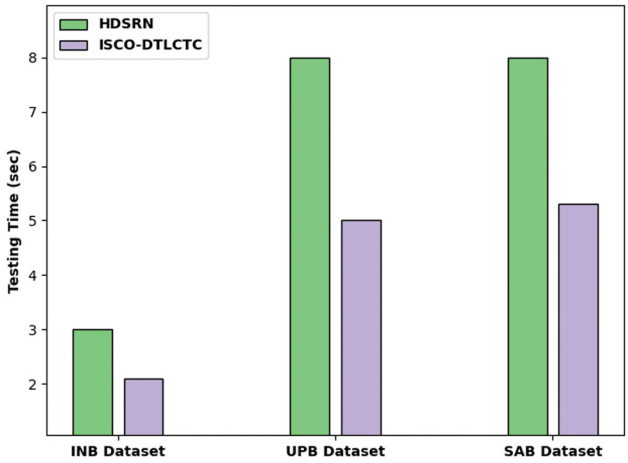

Figure 8. TST analysis of ISCO-DTLCTC technique under 3 datasets.

Table 5. Comparative analysis of ISCO-DTLCTC technique with recent approaches in terms of different measures.

Methods	Overall Accuracy	Average Accuracy	Kappa
INB dataset			
HDSRN	99.70	99.62	99.70
ISCO-DTLCTC	99.85	99.59	99.39
UPB dataset			
HDSRN	99.86	99.84	99.83
ISCO-DTLCTC	99.91	99.88	99.84
SAB dataset			
HDSRN	99.97	99.97	99.97
ISCO-DTLCTC	99.99	99.98	99.98

offered superior TRT of 940 seconds. In addition, with SAB dataset, the ISCO-DTLCTC model has offered lower TRT of 761 seconds , whereas the HDSRN technique has provided higher TRT of 930 seconds.

Figure 8 depicts the comparative TST examination of the ISCO-DTLCTC model with the existing HDSRN model. The figure indicated that the ISCO-DTLCTC model has accomplished enhanced outcomes with the minimal TST under all datasets. For instance, with INB dataset, the ISCO-DTLCTC algorithm has obtainable lower TST of 2.10 seconds, whereas the HDSRN methodology has provided higher TST of 3 seconds. Also, with UPB dataset, the ISCO-DTLCTC model has offered lesser TST of 5 seconds, whereas the HDSRN system has provided higher TST of 8 seconds. Finally, with SAB dataset, the ISCO-DTLCTC technique has offered lower TST of 5.30 seconds, whereas the HDSRN model has provided superior TST of 8 seconds.

Table 5 provides a comprehensive comparative study of the ISCO-DTLCTC model with recent methods in terms of overall accuracy (OACC), average accuracy (AACC), and kappa.

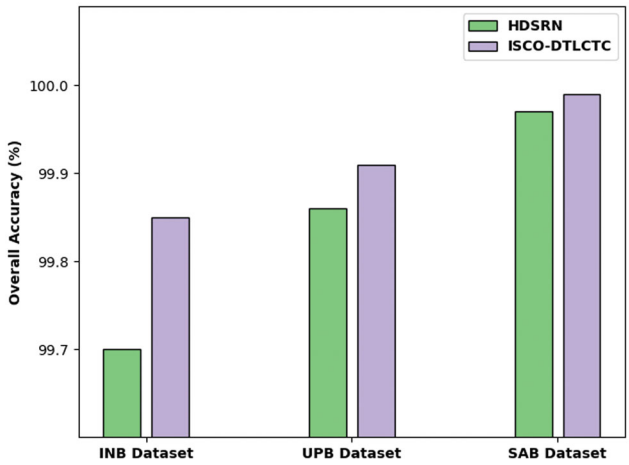

Figure 9. OACC analysis of ISCO-DTLCTC technique with recent approaches.

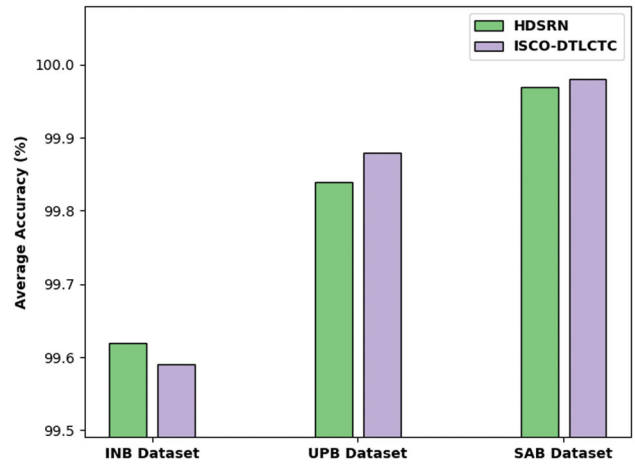

Figure 10. AACC analysis of ISCO-DTLCTC technique with recent approaches.

Figure 9 portrays the OACC results of the ISCO-DTLCTC model with existing method on distinct dataset. The results indicated that the ISCO-DTLCTC model has offered higher OACC compared to HDSRN model on all datasets. For instance, on INB dataset, the ISCO-DTLCTC model has gained increased OACC of 99.85%, whereas the HDSRN model has offered reduced OACC of 99.70%. Similarly, on UPB dataset, the ISCO-DTLCTC model has provided improved OACC of 99.91%, whereas the HDSRN model has resulted in reduced OACC of 99.86%. Moreover, on SAB dataset, the ISCO-DTLCTC model has depicted better OACC of 99.99%, whereas the HDSRN model has provided inferior OACC of 99.97%.

Figure 10 shows the AACC results of the ISCO-DTLCTC model with existing method on distinct dataset. The results exposed that the ISCO-DTLCTC model has offered higher AACC compared to HDSRN model

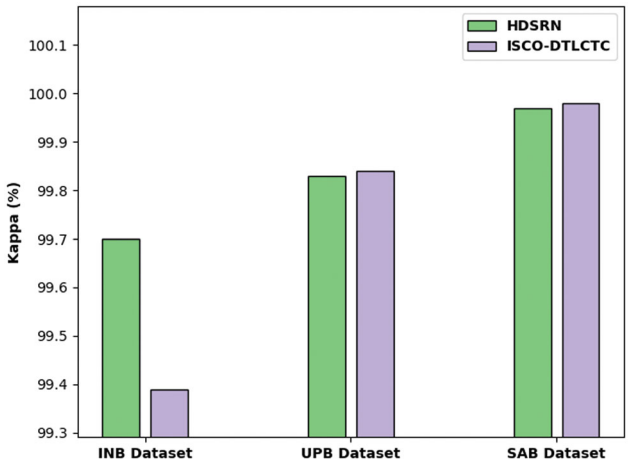

Figure 11. Kappa analysis of ISCO-DTLCTC technique with recent approaches.

on all datasets. For instance, on INB dataset, the ISCO-DTLCTC model has gained increased AACC of 99.59%, whereas the HDSRN approach has obtainable reduced AACC of 99.62%. Similarly, on UPB dataset, the ISCO-DTLCTC model has provided improved AACC of 99.88%, whereas the HDSRN model has resulted in reduced AACC of 99.84%. Moreover, on SAB dataset, the ISCO-DTLCTC system has portrayed better AACC of 99.98%, whereas the HDSRN algorithm has provided inferior AACC of 99.97%.

Figure 11 represents the kappa results of the ISCO-DTLCTC system with existing approach on distinct dataset. The outcomes indicated that the ISCO-DTLCTC approach has offered higher kappa compared to HDSRN model on all datasets. For instance, on INB dataset, the ISCO-DTLCTC model has gained increased kappa of 99.39%, whereas the HDSRN model has offered reduced kappa of 99.70%. Also, on UPB dataset, the ISCO-DTLCTC methodology has provided enhanced kappa of 99.84%, whereas the HDSRN model has resulted in reduced kappa of 99.83%. Furthermore, on SAB dataset, the ISCO-DTLCTC model has depicted better kappa of 99.98%, whereas the HDSRN model has provided inferior kappa of 99.97%.

From the above results and discussion, it is ensured that the ISCO-DTLCTC model can accomplish enhanced performance over the other methods of crop classification process.

Conclusion

In this study, a new ISCO-DTLCTC technique has been developed for the detection and classification of crop types on HRSs. The presented ISCO-DTLCTC technique comprises different stages of subprocesses,

namely, preprocessing, RoI extraction, IGFR-based feature reduction, fusion-based feature extraction, MENN-based crop classification, and SCO-based parameter optimization. The design of SCO algorithm helps to proficiently select the parameters involved in the MENN model and thereby results in improved classification outcomes. The performance validation of the ISCO-DTLCTC model is carried out using benchmark dataset and the results are inspected under several measures. Extensive comparative results demonstrated the betterment of the ISCO-DTLCTC model over the recent state of art approaches. In the future, the ISCO-DTLCTC technique can be deployed for forest fire detection on HRSs. Besides, the performance can be improved by the use of hybrid DL models. In addition, the proposed model can be employed in real time crop type mapping classification on the IoT environment.

Author contributions

The manuscript was written through contributions of all authors. All authors have given approval to the final version of the manuscript.

Data availability statement

Data sharing not applicable to this article as no datasets were generated during the current study.

References

Abualigah, L., and Diabat, A. 2021. "Advances in sine cosine algorithm: A comprehensive survey." *Artificial Intelligence Review*, Vol. 54(No. 4): pp. 2567–2608. doi:10.1007/s10462-020-09909-3.

Ang, K.L.-M., and Seng, J.K.P. 2021. "Big data and machine learning with hyperspectral information in agriculture." *IEEE Access*, Vol. 9: pp. 36699–36718. doi:10.1109/ACCESS.2021.3051196.

Bernardo, L.S., Damaševičius, R., de Albuquerque, V.H.C., and Maskeliūnas, R. 2021. "A hybrid two-stage SqueezeNet and support vector machine system for Parkinson's disease detection based on handwritten spiral patterns." *Advanced Machine Learning Techniques in Data Analysis*. Vol. 31: pp. 549–561.

Bhosle, K., and Musande, V. 2019. "Evaluation of deep learning CNN model for land use land cover classification and crop identification using hyperspectral remote sensing images." *Journal of the Indian Society of Remote Sensing*, Vol. 47(No. 11): pp. 1949–1958. doi:10.1007/s12524-019-01041-2.

Chasmer, L.E., Ryerson, R.A., and Coburn, C.A. 2022. "Educating the next generation of remote sensing specialists: Skills and industry needs in a changing world." *Canadian Journal of Remote Sensing*, Vol. 48(No. 1): pp. 55–70. doi:10.1080/07038992.2021.1925531.

Jamali, A., Mahdianpari, M., Brisco, B., Granger, J., Mohammadimanesh, F., and Salehi, B. 2021. "Wetland mapping using multi-spectral satellite imagery and deep convolutional neural networks: A case study in Newfoundland and Labrador." *Canadian Journal of Remote Sensing*, Vol. 47(No. 2): pp. 243–260. doi:10.1080/07038992.2021.1901562.

Kuo, B.-C., Ho, H.-H., Li, C.-H., Hung, C.-C., and Taur, J.-S. 2014. "A kernel-based feature selection method for SVM with RBF kernel for hyperspectral image classification." *IEEE Journal of Selected Topics in Applied Earth Observations and Remote Sensing*, Vol. 7(No. 1): pp. 317–326. doi:10.1109/JSTARS.2013.2262926.

Lassalle, G. 2021. "Monitoring natural and anthropogenic plant stressors by hyperspectral remote sensing: Recommendations and guidelines based on a meta-review." *The Science of the Total Environment*, Vol. 788(No. September): pp. 147758. doi:10.1016/j.scitotenv.2021.147758.

Lu, B., Dao, P., Liu, J., He, Y., and Shang, J. 2020. "Recent advances of hyperspectral imaging technology and applications in agriculture." *Remote Sensing*, Vol. 12(No. 16): pp. 2659. doi:10.3390/rs12162659.

Luo, F., Du, B., Zhang, L., Zhang, L., and Tao, D. 2019. "Feature learning using spatial-spectral hypergraph discriminant analysis for hyperspectral image." *IEEE Transactions on Cybernetics*, Vol. 49(No. 7): pp. 2406–2419.

Mansour, R., Escorcia-Gutierrez, J., Gamarra, M., Villanueva, J.A., and Leal, N. 2021. "Intelligent video anomaly detection and classification using faster RCNN with deep reinforcement learning model." *Image and Vision Computing*, Vol. 112: pp. 104229. doi:10.1016/j.imavis.2021.104229.

Meneghini, A., Rahimzadeh-Bajgiran, P., Livingston, W., and Weiskittel, A. 2022. "Detecting white pine needle damage through satellite remote sensing." *Canadian Journal of Remote Sensing*, Vol. 48(No. 2): pp. 239–257. doi:10.1080/07038992.2021.2023317.

Nayak, D.R., Padhy, N., Mallick, P.K., Zymbler, M., and Kumar, S. 2022. "Brain tumor classification using dense efficient-net." *Axioms*, Vol. 11(No. 1): pp. 34. doi:10.3390/axioms11010034.

Papp, L., van Leeuwen, B., Szilassi, P., Tobak, Z., Szatmári, J., Árvai, M., Mészáros, J., and Pásztor, L. 2021. "Monitoring invasive plant species using hyperspectral remote sensing data." *Land*, Vol. 10(No. 1): pp. 29. doi:10.3390/land10010029.

Roy, S., Mondal, R., Paoletti, M.E., Haut, J.M., and Plaza, A. 2021. "Morphological convolutional neural networks for hyperspectral image classification." *IEEE Journal of Selected Topics in Applied Earth Observations and Remote Sensing*, Vol. 14: pp. 8689–8702. doi:10.1109/JSTARS.2021.3088228.

Shi, H., Cao, G., Ge, Z., Zhang, Y., and Fu, P. 2021. "Double-branch network with pyramidal convolution and iterative attention for hyperspectral image classification." *Remote Sensing*, Vol. 13(No. 7): pp. 1403. doi:10.3390/rs13071403.

Singh, N., and Singh, P. 2021. "A hybrid ensemble-filter wrapper feature selection approach for medical data classification." *Chemometrics and Intelligent Laboratory Systems*, Vol. 217: pp. 104396. doi:10.1016/j.chemolab.2021.104396.

Singh, P., Pandey, P.C., Petropoulos, G.P., Pavlides, A., Srivastava, P.K., Koutsias, N., Deng, K.A.K., and Bao, Y.

2020. "Hyperspectral remote sensing in precision agriculture: Present status, challenges, and future trends." *Hyperspectral Remote Sensing*, Vol. 2020: pp. 121–146.

Song, Z., and Wang, J. 2021. "Automatic identification of atrial fibrillation based on the Modified Elman Neural Network with exponential moving average algorithm." *Measurement*, Vol. 183: pp. 109806. doi:10.1016/j.measurement.2021.109806.

Sun, H., Zheng, X., Lu, X., and Wu, S. 2020. "Spectral–spatial attention network for hyperspectral image classification." *IEEE Transactions on Geoscience and Remote Sensing*, Vol. 58(No. 5): pp. 3232–3245. doi: 10.1109/TGRS.2019.2951160.

Talkhabi, M., Shamsi, M., and Aghaei, M. 2022. Fruit Recognition and Classification Using Deep Learning (Case Study Date Plant) (No. 7292). EasyChair.

Thenkabail, P.S., Lyon, J.G. and Huete, A. eds., 2018. Advanced Applications in Remote Sensing of Agricultural Crops and Natural Vegetation. CRC press.

Uddin, M.P., Mamun, M.A., and Hossain, M.A. 2021. "PCA-based feature reduction for hyperspectral remote sensing image classification." *IETE Technical Review*, Vol. 38(No. 4): pp. 377–396. doi:10.1080/02564602.2020.1740615.

Wan, S., Yeh, M.-L., and Ma, H.-L. 2021. "An innovative intelligent system with integrated CNN and SVM: Considering various crops through hyperspectral image data." *ISPRS International Journal of Geo-Information*, Vol. 10(No. 4): pp. 242. doi:10.3390/ijgi10040242.

Wei, L., Wang, K., Lu, Q., Liang, Y., Li, H., Wang, Z., Wang, R., and Cao, L. 2021. "Crops fine classification in airborne hyperspectral imagery based on multi-feature fusion and deep learning." *Remote Sensing*, Vol. 13(No. 15): pp. 2917. doi:10.3390/rs13152917.

Zhao, C., Zhao, H., Wang, G., and Chen, H. 2020. "Hybrid depth-separable residual networks for hyperspectral image classification." *Complexity*, Vol. 2020: pp. 1–17. doi:10.1155/2020/4608647.